Assimilation of Tropical Cyclone Track and Structure Based on the Ensemble Kalman Filter (EnKF)

CHUN-CHIEH WU AND GUO-YUAN LIEN

Department of Atmospheric Sciences, National Taiwan University, Taipei, Taiwan

JAN-HUEY CHEN

NOAA/Geophysical Fluid Dynamics Laboratory, Princeton, New Jersey

FUQING ZHANG

Department of Meteorology, The Pennsylvania State University, University Park, Pennsylvania

(Manuscript received 15 January 2010, in final form 12 August 2010)

ABSTRACT

A new tropical cyclone vortex initialization method based on the ensemble Kalman filter (EnKF) is proposed in this study. Three observed parameters that are related to the tropical cyclone (TC) track and structure—center position, velocity of storm motion, and surface axisymmetric wind structure—are assimilated into the high-resolution Weather Research and Forecasting (WRF) model during a 24-h initialization period to develop a dynamically balanced TC vortex without employing any extra bogus schemes. The first two parameters are available from the TC track data of operational centers, which are mainly based on satellite analysis. The radial wind profile is constructed by fitting the combined information from both the best-track and the dropwindsonde data available from aircraft surveillance observations, such as the Dropwindsonde Observations for Typhoon Surveillance near the Taiwan Region (DOTSTAR).

The initialized vortex structure is consistent with the observations of a typical vertical TC structure, even though only the surface wind profile is assimilated. In addition, the subsequent numerical integration shows minor adjustments during early periods, indicating that the analysis fields obtained from this method are dynamically balanced. Such a feature is important for TC numerical integrations. The results here suggest that this new method promises an improved TC initialization and could possibly contribute to some high-resolution numerical experiments to better understand the dynamics of TC structure and to improve operational TC model forecasts. Further applications of this method with sophisticated data from The Observing System Research and Predictability Experiment (THORPEX) Pacific Asian Regional Campaign (T-PARC) will be shown in a follow-up paper.

1. Introduction

Over the past 30 years, track forecasts of tropical cyclones (TCs) have shown steady improvements in accuracy, but initializing a realistic vortex at the correct location with the correct storm motion and structure in the numerical model still remains a challenging task. A TC generally spends most of its lifetime over ocean regions, where conventional observations are sparse, resulting in uncertainty and poor quality in initial conditions and leading to errors in numerical simulations and predictions of TCs. In particular, TC initialization also affects the evolution of TC intensity and inner-core structure. Some techniques, including vortex bogusing (Bender et al.1993; Kurihara et al. 1993, 1995, 1998), bogus data assimilation (Zou and Xiao 2000; Xiao et al. 2000), and relocation (Liu et al. 2002), were designed to improve TC initialization and have produced better simulations of TC movements and structures.

Taking into account a TC's feature of highly rotational and axisymmetric circulations, the conventional vortex bogusing method generally implants a vortex with some reasonable structure at the correct location of the model

Corresponding author address: Chun-Chieh Wu, Dept. of Atmospheric Sciences, National Taiwan University, No. 1, Sec. 4, Roosevelt Rd., Taipei 106, Taiwan.
E-mail: cwu@typhoon.as.ntu.edu.tw

DOI: 10.1175/2010JAS3444.1

initial conditions. Kurihara et al. (1995) had shown that a better prediction could be achieved by the use of improved initialization procedures that better represent the initial environment, the vortex-scale flow, and the mass fields. However, the bogused procedure is rather subjective, and there is no consistent way to implant a bogused vortex so that it is in good agreement with the observations. Moreover, apparent initial adjustments often occur during the spinup period of the numerical integration because of the dynamical imbalance between the vortex and the environmental mass field in the model. In the follow-up to this work, Wu and Huang (2000) showed that numerical simulations of TC track and intensity tend to contain systematic biases, which also vary with different initial conditions.

Based on the four-dimensional variational data assimilation (4D-VAR) framework, Zou and Xiao (2000) proposed a more advanced TC initialization method, called bogus data assimilation (BDA). Further studies (Pu and Braun 2001; Park and Zou 2004; Wu et al. 2006) indicated that the bogus data assimilation could improve TC forecasting and could show more balanced fields than the conventional vortex bogusing method. However, the 4D-VAR calculations take a considerable amount of computation time and may give rise to some computational problems as the model is unable to find the convergent solution when the time frame is too long. In addition, the process of constructing the bogus data remains undetermined.

Considering the use of in situ observations collected by surveillance missions of Dropwindsonde Observation for Typhoon Surveillance near the Taiwan Region (DOTSTAR; Wu et al. 2005), Chou and Wu (2008) proposed a combined initialization method to include both bogusing vortex and dropwindsonde data. Their results showed that the average track and intensity error rates could be reduced in 10 DOTSTAR missions in 2004.

The above research clearly pointed out that the improvement of the initial conditions is crucial for better simulation or prediction of TCs. For an applicable TC initialization scheme, two important properties are required. First, the constructed vortex should be well balanced and dynamically consistent with the numerical model. Second, the method should be able to effectively make use of those key parameters observed for TCs. To meet these two requirements, this study uses a new TC initialization method based on the ensemble Kalman filter (EnKF) to construct suitable TC initial conditions for high-resolution TC simulations. In this paper, the concept of this method is demonstrated. A companion paper (Wu et al. 2010) will discuss how to assimilate The Observing System Research and Predictability Experiment (THORPEX) Pacific Asian Regional Campaign (T-PARC; Elsberry and Harr 2008) data in a continuous update cycle to reconstruct the trajectory of TCs and to study the TC dynamical evolution in more detail.

Regarding the use of the EnKF for TCs, Chen and Snyder (2007) proposed that the observation of TC positions from satellite or radar imagery can be assimilated by the EnKF method in a simple two-dimensional barotropic model given that an operator computes the position of the vortex in the background forecast. Chen and Snyder (2007) further demonstrated that the track initialized with the EnKF analysis is improved and the spurious transient evolution of the initial vortex is reduced. The limitation is that the initial position error has to be comparable to or smaller than the vortex size; otherwise, the non-Gaussian effects become significant while the EnKF's linear update begins to degrade. However, using the observations from satellites, radar, and in situ aircrafts, the TC position error estimated by weather operational centers is about 20 km (Elsberry 1995). Therefore, with accurate and frequent TC observations, the background forecast errors can be limited to a reasonably small range, with acceptable non-Gaussian effect. In other words, Chen and Snyder (2007) showed that the EnKF analysis can be a feasible method to assimilate the TC position data. This was later implemented in a real-data study by Torn and Hakim (2009). On the other hand, with assimilation of abundant inner-core observations such as those from Doppler radars, Zhang et al. (2009) showed that the EnKF can be effective to initialize a TC even without assimilation of the TC position data.

Encouraged by the work of Chen and Snyder (2007), and to help initialize TCs with reasonable track, motion, and mean structure, this study proposes a new approach for a TC initialization procedure by constructing three special observational TC parameters via the EnKF method in the high-resolution Weather Research and Forecasting (WRF) model. The three observational parameters are TC position, the storm motion vector, and the axisymmetric surface wind structure. As is the case with the TC observed positions, the storm motion vector is available from the operational forecast center, which is mainly based on satellite analyses, while the axisymmetric surface wind structure (radial wind profile) is estimated based on the wind radii data from operational centers and the dropwindsonde data, such as those collected in the DOTSTAR program. The EnKF method and the settings of the Advanced Research WRF model (ARW-WRF) are briefly reviewed in section 2. Section 3 describes the designs of three special TC parameters. Section 4 shows the results of the initialization and simulation of Typhoon Fung-wong (2008) based on the proposed EnKF method. Section 5 presents the concluding remarks.

2. Methodology

a. The EnKF data assimilation method

Evensen (1994) first proposed the ensemble Kalman filter (EnKF), which is a better alternative to the traditional Kalman filter because it takes advantage of an ensemble of model states. As in the traditional Kalman filter,

$$\mathbf{K} = \mathbf{P}^f\mathbf{H}^{\mathrm{T}}(\mathbf{H}\mathbf{P}^f\mathbf{H}^{\mathrm{T}} + \mathbf{R})^{-1} \quad \text{and} \tag{1a}$$

$$\mathbf{x}^a = \mathbf{x}^f + \mathbf{K}(\mathbf{y}^o - \mathbf{H}\mathbf{x}^f), \tag{1b}$$

where $\mathbf{x}^a$ is the analysis state vector estimated from the observations $\mathbf{y}^o$ and the background forecasts $\mathbf{x}^f$ in terms of a weighted proportion that is represented by the Kalman gain matrix $\mathbf{K}$. The background-error covariance matrix $\mathbf{P}^f$ contains the error covariances of any two elements of $\mathbf{x}^f$, but it is not actually calculated in the EnKF. Instead, $\mathbf{P}^f\mathbf{H}^{\mathrm{T}}$ and $\mathbf{H}\mathbf{P}^f\mathbf{H}^{\mathrm{T}}$ can be approximated using sample covariances from the ensemble of model forecasts. A complete review of EnKF was documented in Evensen (2003). The practical implementation in this study is similar to the square root version of the EnKF introduced by Whitaker and Hamill (2002). A number of studies (Snyder and Zhang 2003; Zhang et al. 2004, 2006; Zhang and Snyder 2007; Fujita et al. 2008; Meng and Zhang 2007, 2008a,b; Zhang et al. 2009; Torn and Hakim 2009; Yussouf and Stensrud 2010) have showed the potential applications of the EnKF in data assimilation of mesoscale weather systems, including TCs.

The updated equations of the EnKF are valid under the assumptions of the infinite ensemble numbers and the perfect dynamical model. Thus, the insufficiency of ensemble numbers, poor initial ensembles, and errors of the numerical model will result in an analysis ensemble with underestimated error covariances (Burgers et al. 1998). Covariance inflation is often adopted to magnify the variance among the ensemble members of the EnKF analysis. In this study, the analysis ensemble deviation is modified based on the ''covariance relaxation'' method described by Zhang et al. (2004):

$$\mathbf{x}'^a_{(k)\mathrm{new}} = (1-\alpha)\mathbf{x}'^a_{(k)} + \alpha\mathbf{x}'^f_{(k)}, \tag{2}$$

where the parameter α is between 0 and 1. When the value of α is larger than 0, the new analysis ensemble deviation is relaxed toward the prior forecast ensemble deviation $\mathbf{x}'^f_{(k)}$, which is typically greater than $\mathbf{x}'^a_{(k)}$. That is, the covariance inflation would become stronger with the increase of the parameter α. This method differs from the typical covariance inflation method. It shows the advantage that the variance of the analysis is artificially increased only in the regions influenced by the assimilated observations. The horizontal covariance localization method is also used in this study. By multiplying a coefficient that is computed by using Eq. (4.10) of Gaspari and Cohn (1999), the analysis increment is gradually reduced and set to 0 at about 800 km from the TC center.

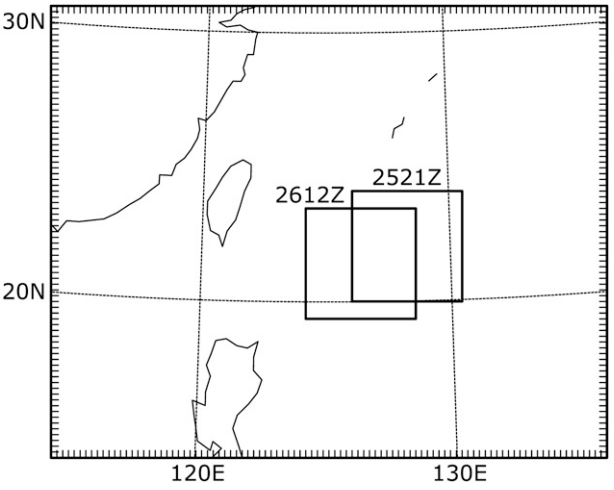

FIG. 1. The nested domains in the experiments of Typhoon Fung-wong. The two squares represent the location and the range of the moveable inner domain at the starting (2100 UTC 25 Jul) and ending (1200 UTC 26 Jul) times of the initialization period.

b. Settings of WRF model and EnKF data assimilation system

The WRF-based EnKF data assimilation system used in this study is similar to the system developed in Meng and Zhang (2008a,b). The ARW-WRF (version 2.2.1) is employed to conduct the numerical simulation. Figure 1 shows the range of the two nested domains used to perform the initialization and forecast experiments of the demonstrated case, Typhoon Fung-wong, starting from 1200 UTC 25 July 2008. The horizontal grid spacing is 24 km (97 × 79 grid points) for the outer domain and 8 km for the moveable inner domain (58 × 58 grid points). The model was run with 35 vertical levels (1.0000, 0.9976, 0.9920, 0.9825, 0.9690, 0.9505, 0.9270, 0.8980, 0.8640, 0.8250, 0.7820, 0.7358, 0.6871, 0.6364, 0.5845, 0.5320, 0.4800, 0.4307, 0.3857, 0.3440, 0.3056, 0.2702, 0.2375, 0.2075, 0.1799, 0.1546, 0.1315, 0.1105, 0.0914, 0.0738, 0.0574, 0.0420, 0.0274, 0.0134, and 0.0000) in the terrain-following sigma coordinate. Note that the two-way vortex-following nest technique is implemented in both forward model simulations and in the EnKF update. Following the TC movement, the moveable inner domain is centered at the TC to ensure that the high-resolution simulation is in the TC core region. The initial and boundary conditions are based on the National Centers for Environmental

Prediction (NCEP) final analysis (FNL) and the optimally interpolated microwave SST (OISST).

The state variables in the WRF model are horizontal and vertical wind fields (u, v, and w), perturbation potential temperature (θ'), perturbation geopotential (ϕ'), and perturbation dry air mass in a column (μ'_d). Moreover, six mixing ratios [water vapor (q_v), cloud water (q_c), cloud ice (q_i), rain (q_r), snow (q_s) and graupel (q_g)] are also included to correspond to the choice of the WRF Single Moment (WSM) six-class graupel microphysics scheme (Hong et al. 2004; Hong and Lim 2006). The above state variables will be updated in the EnKF calculation. Other parameterization schemes used in the model include the Rapid Radiative Transfer Model (RRTM) scheme (Mlawer et al. 1997) for longwave radiation, the simple shortwave scheme (Dudhia 1989) for shortwave radiation, and the Yonsei University (YSU) planetary boundary layer scheme (Hong et al. 2006). The cumulus convection is parameterized with the Grell–Devenyi ensemble scheme (Grell and Dévényi 2002) only in the coarser (outer) domain.

Taking NCEP FNL at 1200 UTC 25 July 2008 as the initial ensemble mean, the ensemble members are produced by randomly perturbing the mean analysis. As in Meng and Zhang (2008a,b), the initial perturbations are performed on a transformed streamfunction field in the WRF variational data assimilation system (WRF-Var; Barker et al. 2004), and the background error covariances of WRF-Var are also used. This method guarantees that the horizontal wind (u and v), temperature (T), and pressure perturbations (p') of the initial perturbation field are in geostrophic balance (Barker et al. 2003; Zhang et al. 2006). The other state variables, such as vertical wind and mixing ratios, are not perturbed here.

3. Descriptions of the three special TC parameters

In this study, three special observational parameters of TCs are assimilated via the EnKF method: the TC center position, the storm motion vector, and the axisymmetric surface wind structure. These three parameters are generally used to describe the track and structure of a TC but have not been adopted in the existing TC data assimilation system. A common property of these parameters is that they are usually obtained by combining different kinds of observations. Therefore, the adoption of these parameters as ''observables'' in data assimilation is not a straightforward process. In addition, the observation operators used to convert the model variables to these three parameters are usually highly nonlinear. However, in the EnKF method, the ensemble covariance not only efficiently provides the error covariance of the state variables, but also allows for the nonlinear observation operator. Therefore, the above three special observational parameters can be easily assimilated into the model by the EnKF technique.

Assimilating the TC center position and the storm motion vector is assumed to help correct the TC track and maintain reasonable storm movement. Also, assimilating the axisymmetric surface wind structure is assumed to help construct a TC-like vortex with reasonable structure, although only a one-dimensional wind profile extracted from a three-dimensional wind field is assimilated here. It is not difficult to obtain this representative mean profile despite limited observations. Furthermore, an experiment demonstrated later shows that a reasonable vertical TC structure can be successfully established through the assimilation of only these data by the EnKF method. The detailed usage of the three parameters is described in the following subsections.

a. TC center position

The observed TC center position of Typhoon Fungwong is obtained from the TC position data of the Central Weather Bureau (CWB) of Taiwan analyzed at 3-h intervals. The cubic spline algorithm is used to interpolate the data into 30-min intervals for the EnKF update cycle. Considering the operational analysis errors of TC position (Edson and Lander 2003) and the performances of several EnKF assimilation tests, in this study the observation errors of the TC location in both the latitudinal and the meridional directions are set at 20 km at the beginning of the initialization period and gradually decrease to 13 km by the end [composite TC location error (i.e., multiplied by square root of 2) is shown as the dotted line in Fig. 8]. Tests of different observation errors were conducted, which showed generally consistent results (figures not shown).

The observation operator used to transfer the geopotential height (Φ) to the TC center on the grid coordinate is shown as

$$i_{\mathrm{TC}} = \frac{\sum_{n=1}^{N} w_n i_n}{\sum_{n=1}^{N} w_n}, \quad j_{\mathrm{TC}} = \frac{\sum_{n=1}^{N} w_n j_n}{\sum_{n=1}^{N} w_n}, \tag{3a}$$

$$\text{where} \quad w_n = \begin{cases} \overline{\langle \Phi \rangle} - \langle \Phi_n \rangle, & \langle \Phi_n \rangle < \overline{\langle \Phi \rangle} \\ 0, & \langle \Phi_n \rangle \geq \overline{\langle \Phi \rangle} \end{cases}. \tag{3b}$$

Here the latitudinal and meridional coordinates of grid points are represented by i and j, respectively; also, $\langle \Phi \rangle$ represents the vertically averaged geopotential height

from 900 to 700 hPa, and $\overline{\langle\Phi\rangle}$ is the mean of a 300 km × 300 km square centered at the local minimum of $\langle\Phi_n\rangle$ adjacent to the reference TC center. The weighted summation is done across each grid point within the above mean area, but only the positive weights (where $\langle\Phi_n\rangle$ is lower than its areal mean value) are taken into account [see Eq. (3b)]. The subscript n indicates each grid point within this area.

b. The storm motion vector

The storm motion vector is derived from the TC center position associated with both observations and the dynamics model based on the same equation:

$$i'_{\mathrm{TC}} = \frac{i_{\mathrm{TC}} - i_{\mathrm{TC,prev}}}{\Delta t}, \quad j'_{\mathrm{TC}} = \frac{j_{\mathrm{TC}} - j_{\mathrm{TC,prev}}}{\Delta t}. \qquad (4)$$

Thus, the above equation is used both to calculate the TC observed position and as the observation operator. The time interval (Δt) between the latest TC center location (i_{TC}, j_{TC}) and the previous one ($i_{\mathrm{TC,prev}}$, $j_{\mathrm{TC,prev}}$) is 3 h. The observation error of the storm motion vector is set to be a constant of 1.5 m s^{-1}, which is based on the performances of several EnKF assimilation tests.

c. The axisymmetric surface wind structure

The axisymmetric surface wind structure of a TC is usually dictated by its azimuthal mean of the tangential wind speed. In most of the idealized numerical experiments, as well as in some of the traditional vortex initialization schemes, a (modified) Rankine vortex wind profile is usually used and bogused to construct the TC structure. This oversimplified TC structure is considerably different from the real TC in the near-core region, which is characterized by relatively slow tangential wind decay in conjunction with a skirt of significant cyclonic relative vorticity that possesses a negative radial gradient (Mallen et al. 2005). To find a reasonable axisymmetric mean wind structure to be assimilated, an empirical formula from Willoughby et al. (2006) is employed (see the appendix) in this study.

Based on the information of the analyzed radii of the 34- and 50-kt winds from the Joint Typhoon Warning Center (JTWC) best-track database (averaged among four different quadrants if the TC has asymmetric wind radii), and the in situ 10-m height surface wind from dropwindsonde data of the DOTSTAR mission, the Willoughby sectionally continuous wind profile [Eqs. (A1)–(A3)] can be determined [$V_{\max}$ = 28 m s^{-1}, $R_{\max}$ = 45 km, X_1 = 480 km, and A = 0.1 based on all available observations; n = 0.729, X_2 = 40 km, and $R_1 = 0.3R_{\max}$ based on the statistics of Willoughby et al. (2006); and R_2 is directly determined by satisfying Eq. (A3)]. The axisymmetric surface wind structure at 1200 UTC 26 July is shown in Fig. 2a. Figure 2b shows brightness temperatures from a polar-orbiting satellite by superposing the flight path and the deployed locations of the dropwindsondes in DOTSTAR of Typhoon Fung-wong at 1200 UTC 26 July 2008. The first and last dropwindsondes reached the surface at 0921 and 1349 UTC, respectively (the summary of this mission can be found on the DOTSTAR

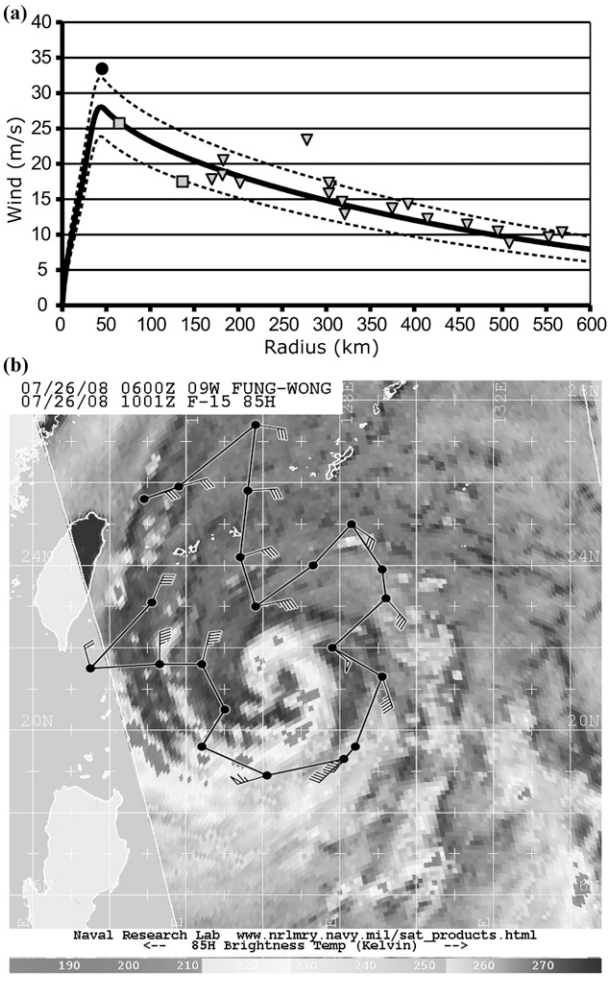

FIG. 2. (a) The axisymmetric surface wind structure at 1200 UTC 26 Jul of Typhoon Fung-wong calculated by the Willoughby sectionally continuous wind profile (thick solid line; $V_{\max}$ = 28 m s^{-1}, $R_{\max}$ = 45 km, n = 0.729, X_1 = 480 km, A = 0.1, R_1 = 13.5 km, and R_2 = 59.8 km). The 10-m surface winds from dropwindsonde data of the DOTSTAR mission are represented by the inverted triangles. The JTWC analyzed the maximum wind. The radii of the 34- and 50-kt wind averaged among four different quadrants are marked by circles and squares, respectively. Dashed lines represent the wind profile plus–minus one observation error computed by Eq. (5). (b) The brightness temperature (K) from a polar-orbiting satellite, superposing the flight path and the deployed locations of the dropwindsondes in DOTSTAR of Typhoon Fung-wong at 1200 UTC 26 Jul.

Web site; see http://typhoon.as.ntu.edu.tw/DOTSTAR/en/flight.php?id=31.) This calculated wind profile is smoother than the dropwindsonde measurement but retains the main characteristics of the azimuthal-mean tangential wind of the real TC.

About 30 samples within the 400-km radius from the calculated wind profile are assimilated by the EnKF method. The interval between the two samples is 20 km for the outer area, and this interval gradually shortens as it approaches the TC center. The lowest half level of the WRF model is set at $\eta = 0.9988$, which is equivalent to the height of about 10 m, for the convenience of constructing the relevant observation operator (10-m wind). One of the unique features in this new method is that while the axisymmetric tangential part of the winds is assimilated, the nonaxisymmetric part is free to develop in the model to be dynamically consistent with any environmental condition (including the asymmetric winds or the background vertical shear) it is embedded in.

Note that since the method of assimilating the above mean wind profile is newly proposed, there are no references available on how to estimate the observation error of the azimuthal-mean tangential wind. Here the observation error of the azimuthal-mean tangential wind is represented by the empirical formula below:

$$R_v(r) = \sqrt{0.5^2 + \{0.4[V(r)]^{0.7}\}^2}. \quad (5)$$

Note that $V(r)$ is the azimuthal-mean tangential wind from Willoughby's sectionally continuous wind profile, and $R_v(r)$ is the observation error of wind speed at radius r. The empirical formula suggests that $R_v(r)$ generally increases with wind speed and reaches a minimum value of 0.5 m s^{-1} when the azimuthal-mean flow is at rest. The power of 0.7 in the formula is arbitrary and its impact on the results of the data assimilation can be examined in a separate study. Our current analysis indicates that the currently used power of 0.7 provides rather reasonable results.

Other than the dropsonde observations, one may adopt other types of available observations to determine the radial wind profile, such as satellite scatterometer winds [e.g., Quick Scatterometer (QuikSCAT)], flight-level or sea surface winds from reconnaissance missions, or even only the limited information provided by operational centers based on satellite analyses (such as the Dvorak technique). The procedure to adopt the special TC parameters for assimilation can be flexible depending on the characteristics and the accuracy of the observations that are utilized. It is noteworthy that the observation error of axisymmetric tangential wind [Eq. (5)] will be larger when no aircraft observations are available in most cases during the analysis time.

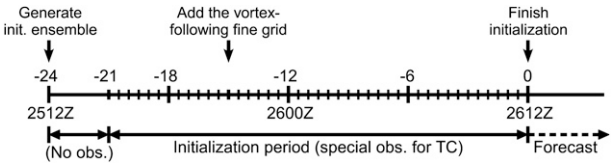

FIG. 3. The time-by-time procedures of the initialization of Typhoon Fung-wong.

4. Results

The method proposed above is demonstrated here for the case of Typhoon Fung-wong (1200 UTC 24 July–1800 UTC 28 July 2008). Figure 3 provides an example of the time-by-time procedures. The 28 ensemble members are generated at 1200 UTC 25 July, which is 24 h before the initial time of the model forecast. During the incipient 3-h simulation, only the outer domain is used without any EnKF assimilation. From 1500 UTC 25 July to 1200 UTC 26 July, the EnKF update cycle is conducted every 30 min to assimilate the three special TC parameters, while the moveable inner domain (following the TC center) is activated at 2100 UTC 25 July. After the 21-h initialization by the EnKF assimilation, a 48-h forecast of Fung-wong follows, with a starting time of 1200 UTC 26 July.

Three numerical experiments are implemented to examine the impact of assimilating the special observational TC parameters. The control experiment (CTL) assimilates all of the three special parameters, while "TK" assimilates only the TC center position and the storm motion vector and "NONE" denotes the experiment without any data assimilation performed. For all experiments, the number of ensemble members is 28, and the covariance relaxation parameter (α) is 0.8.

a. CTL and NONE experiments

Figure 4a shows the TC tracks from the different ensemble members during the 21-h initialization of the CTL experiment. A deviation from the observation track can be found in the incipient 9 h. After executing several EnKF update cycles, the mean track is aligned with the observations and is consistent with the observation track from 0000 to 1200 UTC 26 July. Note that the initial condition is obtained from the NCEP FNL, which is a global model with horizontal resolution of 1° of latitude by 1° of longitude. Thus, the large shift in the beginning is likely attributed to the initial location error, plus the incorrect large-scale steering flow represented in the global analysis. When the assimilation of TC track and structure starts, the increments between observations are too large to obtain an optimized analysis. As a result, it takes several update cycles to correct the analysis position (Chen and Snyder 2007). The surface wind, sea level pressure

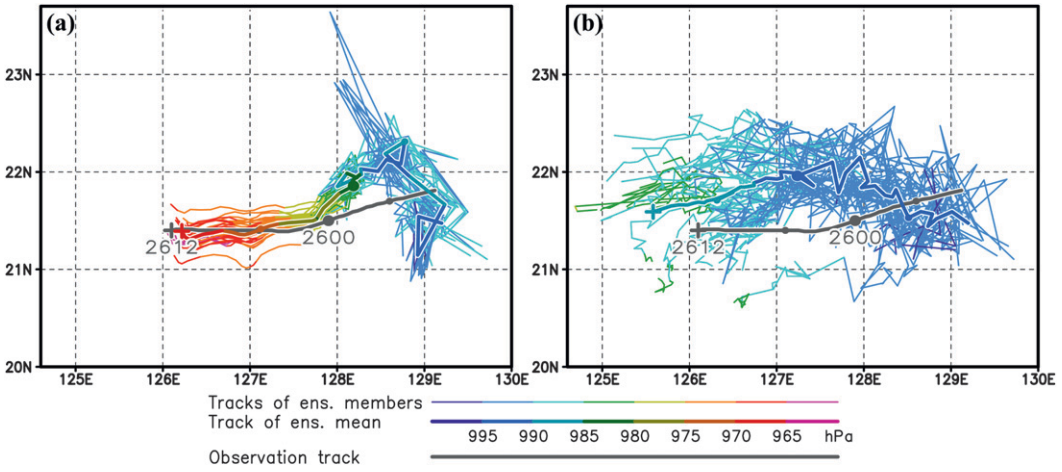

FIG. 4. The ensemble mean track (thick colored line) and the tracks of ensemble members (thin colored lines) with the corresponding SLP shown by colors (hPa) during the 21-h initialization of the (a) CTL and (b) NONE experiments. The thick gray line represents the observation track. Each symbol (crosses and circles) is plotted at 6-h intervals.

(SLP), and axisymmetric wind structure of CTL at the beginning (1500 UTC 25 July), middle (0000 UTC 26 July), and final (1200 UTC 26 July) times of the initialization period are shown in Fig. 5. It can be found that the low-level circulation of the TC becomes stronger in time (Figs. 5a,c,e), whereas the radius of the maximum wind decreases (Figs. 5b,d,f). Furthermore, the mean surface tangential wind structure gradually approaches the wind profile derived from the sectionally continuous wind formula of Willoughby, which fits with the observations (Figs. 5b,d), especially at the end of the initialization period (Fig. 5f).

In contrast, without assimilating any special observational TC parameters, the ensemble tracks of NONE show large deviations from the observation track, as well as large spreads (Fig. 4b). By examining the surface wind and SLP fields (Figs. 6a,c,e), it can be shown that although the TC intensity increases slowly, the TC structure is not well organized throughout the initialization period. The radius of the maximum wind remains unchanged as well (Figs. 6b,d,f). Note that the difference between the model and the observed TC intensity remains large at the end of the initialization period (Fig. 6f).

Figure 7 shows the Hovmöller diagrams (radius–time) of the average surface tangential wind and the minimum SLP of both the CTL and NONE experiments during the initialization period. For the CTL experiment, the surface winds grow stronger while the radius of the maximum wind contracts in time (Fig. 7a). The minimum SLP also deepens from 995 to 970 hPa (Fig. 7b), indicating that the structure of Fong-wong becomes increasingly organized. In contrast, for NONE, the surface wind speed only increases slightly during the initialization period (Fig. 7c), while the minimum SLP deepens only to 987 hPa (Fig. 7d).

The above results demonstrate that the assimilation of special observational parameters can significantly improve track and structure evolution. When only NCEP FNL and OISST data are adopted as the initial conditions without employing additional data assimilation, the TC structure and intensity cannot be well developed during the first 24 h in the high-resolution WRF model run (i.e., the NONE experiment). However, through the EnKF method proposed in this study, a reasonable initial TC vortex can be effectively produced (i.e., the CTL experiment) and used for the follow-up simulation.

Note that the track and surface wind variances among the ensemble members do not expand in time but rather shrink to nearly a constant during the initialization period (Figs. 4a and 5b,d,f). This is because the EnKF update cycle tends to reduce the analysis error covariance. In other words, through the EnKF method, the special observational parameters are well assimilated into the WRF model. The larger minimum SLP variance in the late initialization period of Fig. 7b is perhaps related to the nonlinear relationship between the minimum SLP and TC intensity, as well as to a decoupling between the wind profile and the TC intensity.

To further examine the characteristics of the ensemble during the assimilation, for the TC position, the ensemble mean error measured by the distance from the analysis (forecast) ensemble mean to the observation and the ensemble spread measured by the sample standard deviation of the analysis (forecast) ensemble are calculated by

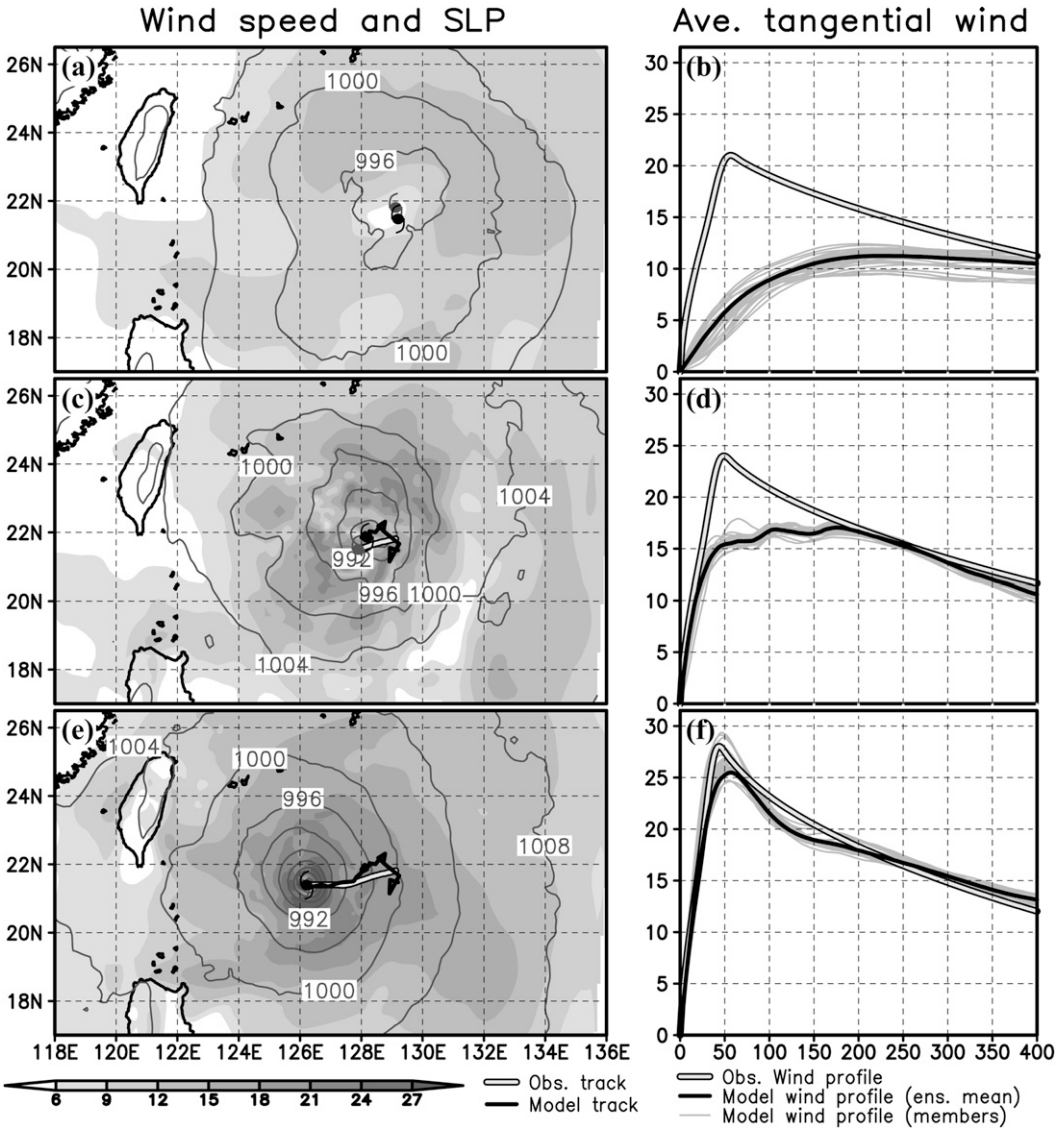

FIG. 5. (a),(c),(e) The surface wind (shaded; m s^{-1}) and sea level pressure (contour; hPa) of CTL at (a) 1500 UTC 25 Jul, (c) 0000 UTC 26 Jul, and (e) 1200 UTC 26 Jul superposing the observed track (double line and typhoon symbol) and the model track (thick black line and typhoon symbol) of CTL from the beginning of the initialization. (b),(d),(f) The corresponding axisymmetric wind profiles of the ensemble mean (thick black line) and each ensemble member (thin gray lines) of CTL and the observed surface tangential wind structures (double line) at the three times (m s^{-1}).

$$d_{\text{pos}}^{a(f)} = \sqrt{[i_{\text{TC}}^{o} - \bar{i}_{\text{TC}}^{a(f)}]^2 + [j_{\text{TC}}^{o} - \bar{j}_{\text{TC}}^{a(f)}]^2} \quad \text{and} \tag{6}$$

$$\sigma_{\text{pos}}^{a(f)} = \left\langle \frac{1}{K-1} \sum_{k=1}^{K} \{[i_{\text{TC}}^{a(f)} - \bar{i}_{\text{TC}}^{a(f)}]^2 + [j_{\text{TC}}^{a(f)} - \bar{j}_{\text{TC}}^{a(f)}]^2\} \right\rangle^{1/2}. \tag{7}$$

Here, $i_{\text{TC}}^{a(f)}$ and $j_{\text{TC}}^{a(f)}$ are the coordinates of the TC center computed from the model analysis (forecast) field with the same definition in Eq. (3), while the bar is used to represent the ensemble mean, and i_{TC}^{o}, j_{TC}^{o} are the assimilated observations. Similarly to the TC position, the ensemble mean error and spread of the axisymmetric surface wind speed can be calculated by

$$d_{\text{wind}}^{a(f)} = \frac{1}{400} \int_0^{400} d_V^{a(f)}(r)\, dr = \frac{1}{400} \int_0^{400} \left| V^{o}(r) - \overline{V^{a(f)}(r)} \right| dr \quad \text{and} \tag{8}$$

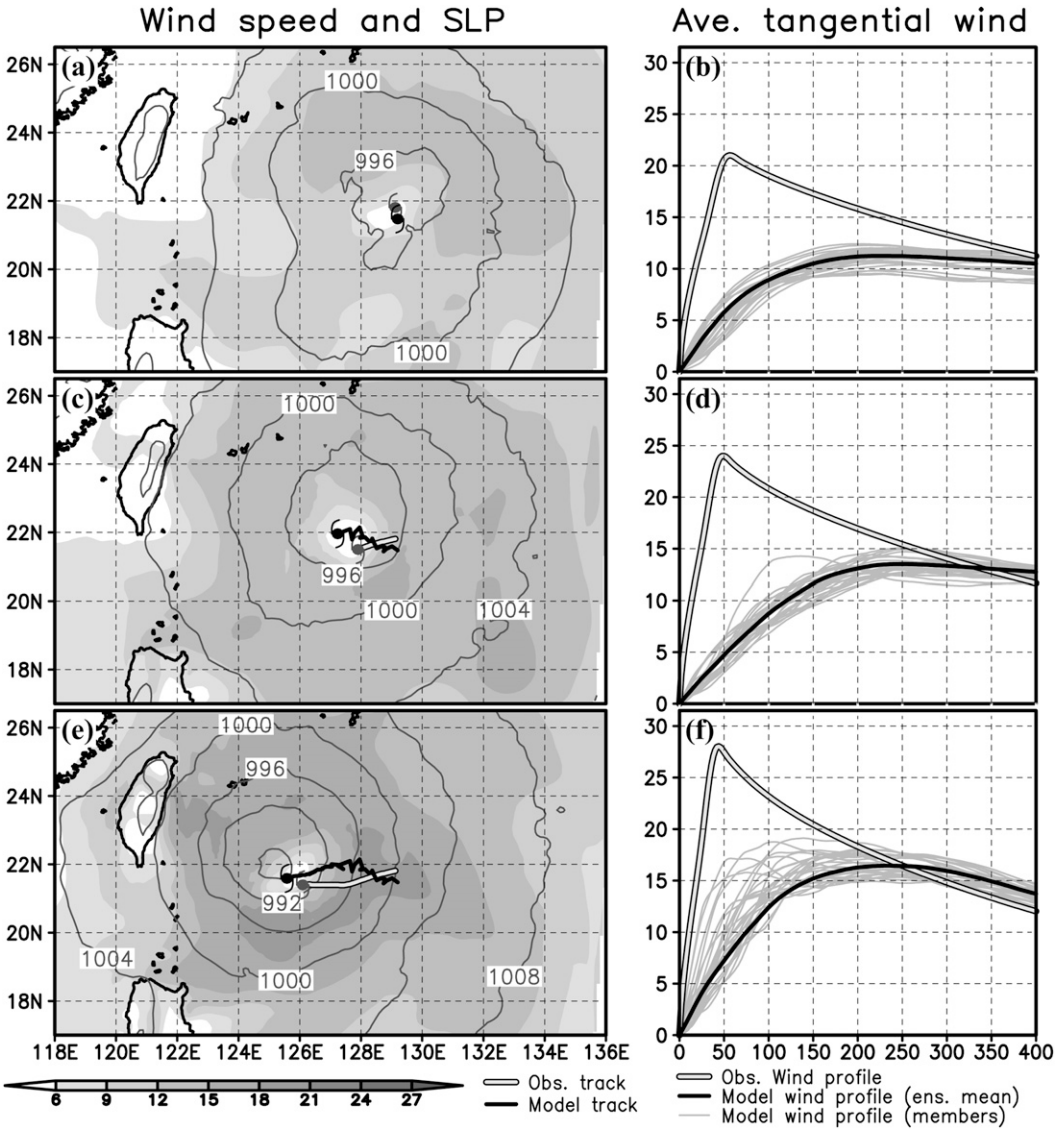

FIG. 6. As in Fig. 5, but for the NONE experiment.

$$\sigma_{\text{wind}}^{a(f)} = \frac{1}{400}\int_0^{400} \sigma_V^{a(f)}(r)\,dr = \frac{1}{400}\int_0^{400}\left\{\frac{1}{K-1}\sum_{k=1}^{K}\left[V^{a(f)}(r) - \overline{V^{a(f)}(r)}\right]^2\right\}^{1/2} dr. \quad (9)$$

Note that the averaged deviation between two wind profiles is defined by the integration of the differences along the radius of 0–400 km. Figure 8 shows their evolution during the assimilation. In CTL, the analysis and forecast ensemble mean error as well as the spread all tend to decrease when the EnKF assimilation starts from 2100 UTC 25 July (Figs. 8a,d). During the last 6 h of the initialization, the forecast and analysis ensemble mean errors of the TC position (thin lines in Fig. 8a) are 13.8 and 9.5 km on average, while their spreads (thick lines in Fig. 8a) are 13.5 and 11.5 km, respectively. For the axisymmetric surface wind, the forecast and analysis ensemble mean errors (thin lines in Fig. 8d) are 1.23 and 1.10 m s^{-1} on average, while their spreads (thick lines in Fig. 8d) are 0.53 and 0.57, respectively, within the last 6 h of the initialization. The above values of errors and spreads are comparable in magnitude with the given observation errors. It can also be noted that the values of analysis errors and spreads (dashed lines) are lower than those associated with forecasts (solid lines) most

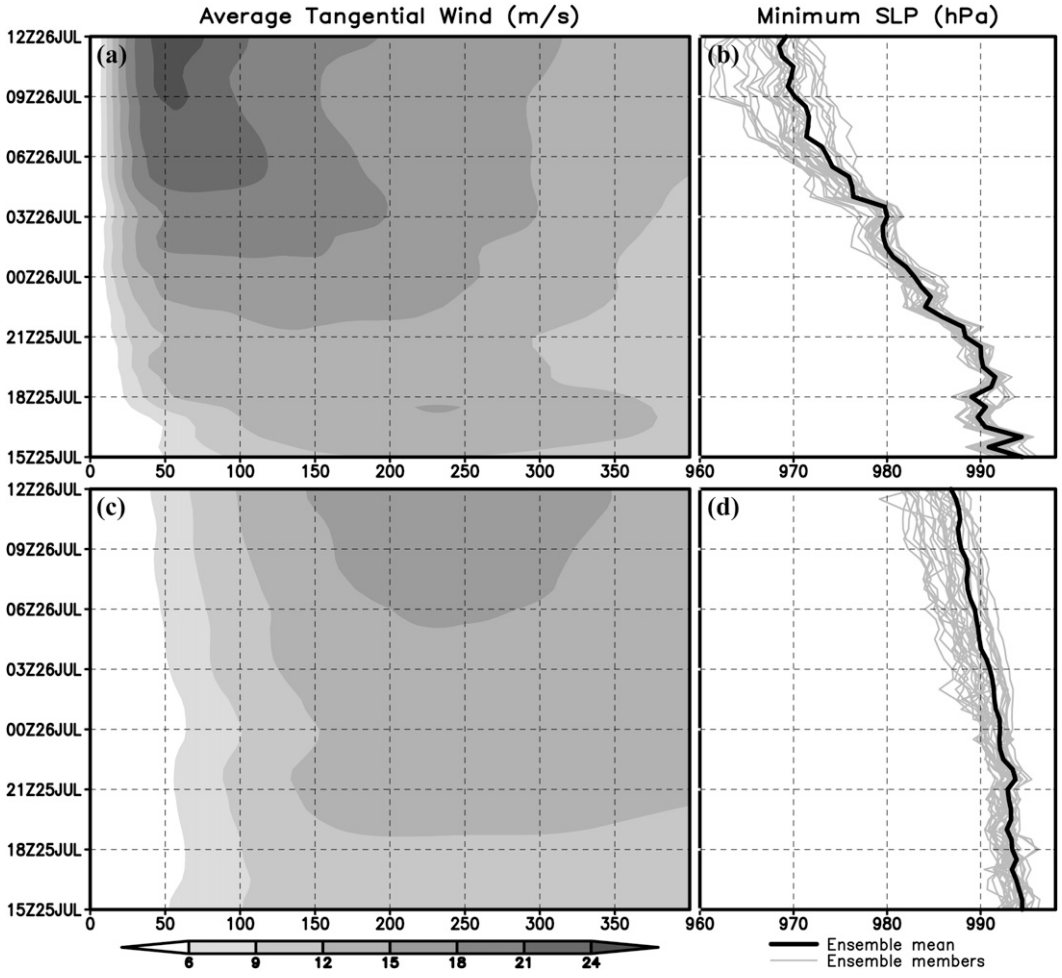

FIG. 7. The Hovmöller diagrams of the azimuthal mean of the tangential wind speed (shaded; m s^{-1}; the x axis is radius) and the minimum SLP (hPa) of the ensemble mean (thick black line) and members (thin gray lines) for both the (a),(b) CTL and (c),(d) NONE experiments during the initialization period.

of the time, which is consistent with the basic concept of the Kalman filter. In contrast, for NONE, the forecast ensemble mean errors of both the TC position and the axisymmetric surface wind are much larger because no observations have been assimilated during the initialization (Figs. 8b,e). (The analysis ensemble mean error in NONE does not exist because no data assimilation is performed during the initialization.)

b. TK experiment

Considering the impacts of the observational TC parameters associated with the TC movements, the TK experiment is conducted for the sole purpose of only assimilating the TC position and the storm motion vector. Its simulated track is consistent with the observation track during the initialization, and the track error is less than 20 km in the final 6 h (thin lines in Fig. 8c). These characteristics are similar to the results of CTL. The ensemble spreads of the TC positions are slightly larger than in CTL (thick lines in Fig. 8c) but are still within the range of 30 km in the final 6 h. In contrast, the TC structure is not well organized until the end of the initialization and the SLP is only 985 hPa (figures not shown), which is similar to the results of NONE. Note that the analysis and forecast ensemble mean errors of the axisymmetric surface wind are almost the same and remain relatively large throughout the initialization period (thin lines in Fig. 8f). This means that the assimilation of the TC position and the storm motion vector does not show any crucial impacts on the near-surface wind field structure.

It is of interest to ask whether the assimilation of the storm motion vector provides additional impacts. To examine this, an extra experiment is conducted without assimilating the storm motion vector. Although the result

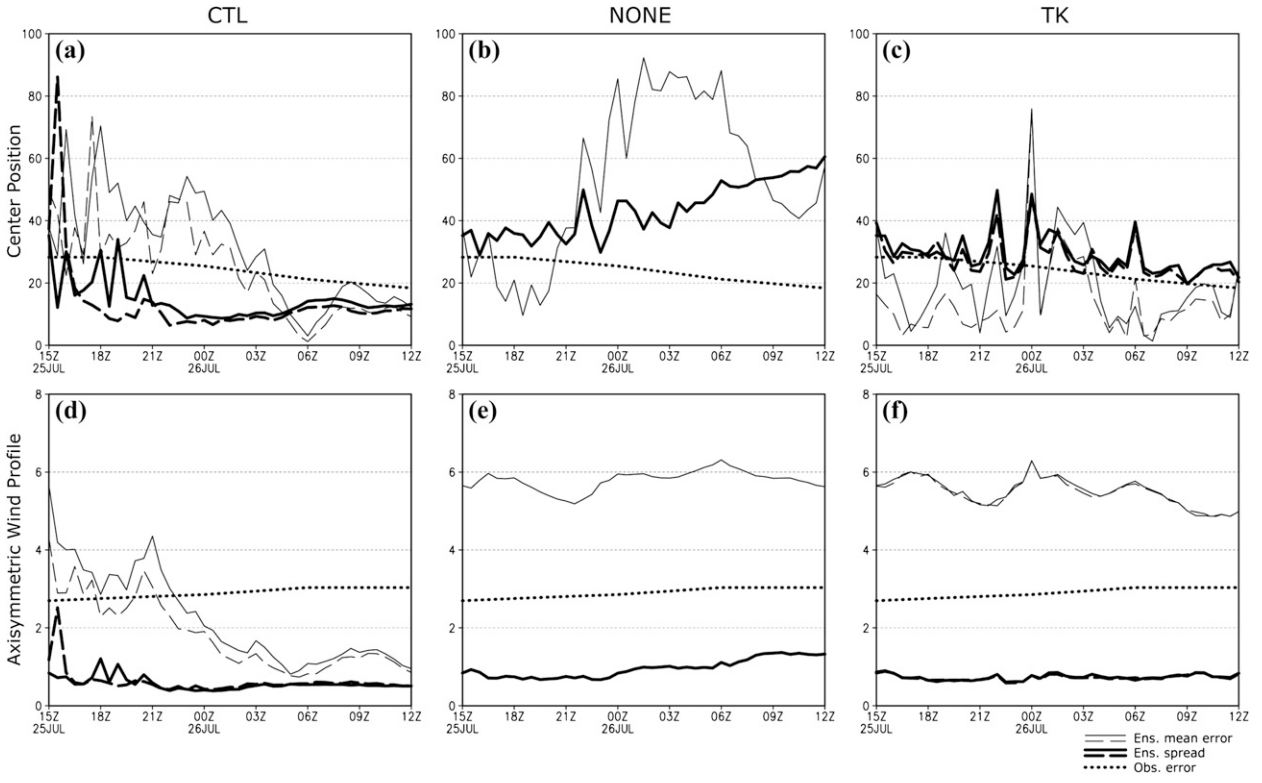

FIG. 8. The ensemble mean error (thin lines) and spread (thick lines) of (a)–(c) the TC center position (km) and (d)–(f) the axisymmetric surface wind profile (m s^{-1}) for the (a),(d) CTL, (b),(e) NONE, and (c),(f) TK experiments. For both thin and thick lines, all solid lines denote those in background forecasts, and all dashed lines denote those in analyses after the EnKF update. The observation errors used in the assimilation are represented by dotted lines.

(not shown) indicates that the mean position error in the extra experiment is nearly the same as that in TK, it can be found that the ensemble spread is larger than that in TK. Therefore, despite the fact that the assimilation of the storm motion vector does not directly reduce the position error, when the assimilation is given frequent position observations, it shows certain impacts on the model state.

On the other hand, the assimilation of the axisymmetric surface wind profile changes neither the TC position nor the mean flow. Unlike other observations, these quantities do not include latitude/longitude information. Therefore, these observations can only correct the structure of the TC, and their impact on TC tracks is also assumed to be minimal. However, in practice, if the TC location is not assimilated, the TC centers of each ensemble member tend to spread out quickly. As a result, it is technically difficult to calculate the average tangential wind profile corresponding to a fixed center position.

c. *Vertical structure*

The vertical structures of the three experiments at the end of initialization are shown by their cross sections of the wind, potential vorticity, and potential temperature fields across the storm center (Fig. 9). In CTL (Fig. 9a), the inner core structures are well established, while the maximum potential vorticity is located at the TC center and the warm-core structure is shown in the middle to upper levels. The surface wind flows inward and ascends upward slantwise to construct the secondary circulation of the TC. By contrast, in NONE and TK (Figs. 9b,c), the secondary circulations are asymmetric, while the potential vorticity and warm-core structure are not apparent.

These vertical structures indicate that even though only surface wind data on a single level are assimilated, a reasonable three-dimensional vertical TC structure can be successfully established by the EnKF method. It is believed that both the data assimilation itself and the subsequent model integration play some role in building up the model vortex and the upper-level warm-core structure. To evaluate the relative contribution of these two effects, the time evolutions of 500-hPa temperature perturbations in the TC center (the difference to the 400-km-radius azimuthal mean) before and after the data assimilation are plotted in Fig. 10. After some incipient undulations, the warm anomaly in the TC center strengthens gradually (Fig. 10a). The increment due to

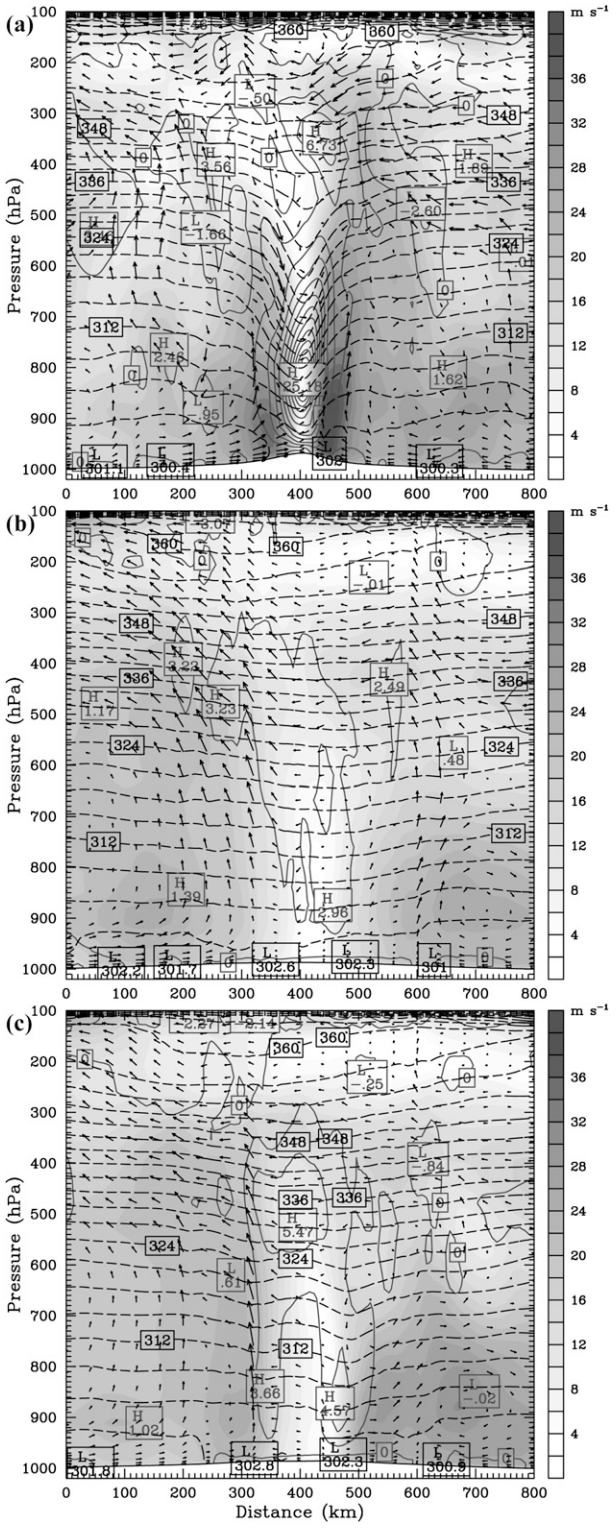

FIG. 9. West–east section through the storm center of horizontal wind speed (shaded; m s^{-1}), potential vorticity (solid contour; PVU), potential temperature (dashed contour; K) and vertical circulation (arrows) of the ensemble mean for the (a) CTL, (b) NONE, and (c) TK experiments.

the data assimilation (difference between the analysis and background forecast fields; dashed line in Fig. 10b) is generally positive after 1900 UTC 25 July, indicating that the assimilation of the surface wind profile directly results in an increase of the upper-level temperature field. However, the increment after the 30-min model integration (difference between the model forecasts and the analyses in the previous update cycle; solid line in Fig. 10b) also has some significant impacts, suggesting that the changed fields in the previous EnKF update cycle can also influence the warm core structure through the following model integration.

d. Forecast results

After the initialization period in CTL, the 48-h model forecast is started from 1200 UTC 26 July. Figure 11 shows the ensemble forecast tracks during both the initialization and the forecast periods of CTL. It can be found that the variance among the ensemble members increases gradually during the forecast period, indicating the uncertainty range of the track forecasts. Despite the effective track assimilation during the initialization period, in this particular case the storm deflects to the north during the initial 18 h of the forecast period (1200 UTC 26 July–0600 UTC 27 July). Note that in this study other available data (such as conventional rawinsondes) have not been used during the 24-h assimilation period, thus somehow resulting in partial loss of the forecast skill. This is probably one of the major reasons why even though the initial condition has been improved through the three parameters, the later forecast in CTL is not much better when compared to that in NONE (not shown). In companion works (Wu et al. 2010; Huang et al. 2010), both the special TC parameters and conventional rawinsonde and dropwindsonde data for Typhoon Sinlaku (2008) during T-PARC are assimilated to keep updating the environmental information.

As for the intensity forecast of Typhoon Fung-wong, Fig. 12 is the minimum SLP at the storm center and the maximum sea surface wind speed during the 48-h forecast from the ensemble mean. It shows that during the first few hours, the TC intensity of CTL is not only close to the observations, but also fairly steady without any spurious adjustments, implying that the model initial condition constructed by the EnKF method is well balanced and dynamically consistent with the model. It is interesting to note that the simulated intensity matches well with the analysis data of CWB during the most intense phase around 27 July, yet the minimum SLP is off by about 20 hPa. This inconsistency may be due to the uncertainty in the wind and pressure analyses in the CWB data. The initial TC intensity of NONE is much weaker than the observations but also reaches an intensity level nearly equivalent to that of

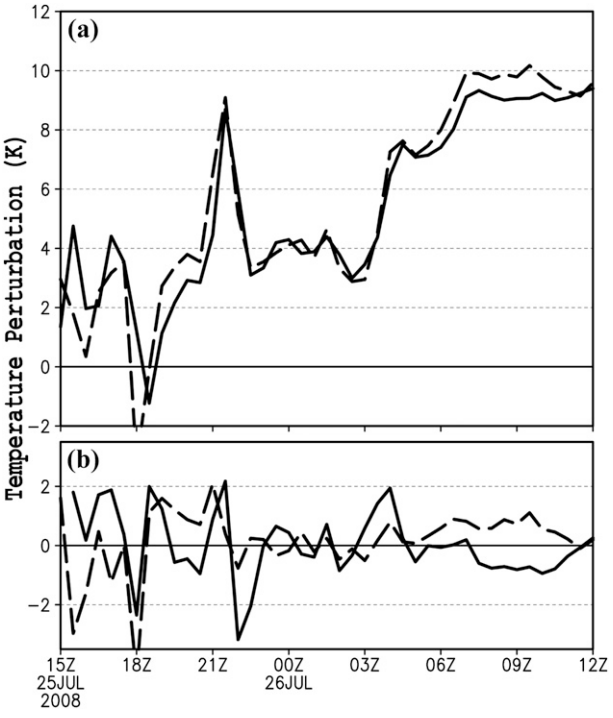

FIG. 10. (a) The time evolutions of 500-hPa temperature perturbations (K) in the TC center (the difference to the 400-km-radius azimuthal mean) in background forecasts (solid line) and in analyses after the EnKF update (dashed line) during the initialization period. (b) As in (a), but for the difference between the analyses and background forecasts (the increment by the data assimilation; dashed line) and for the difference between the model forecasts and the analyses in the previous update cycle (the increment by 30-min model integration; solid line).

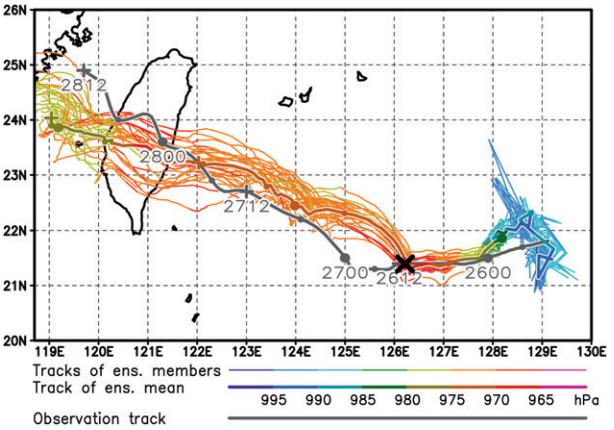

FIG. 11. As in Fig. 4a, but for both initialization and forecast periods (1200 UTC 25 Jul–1200 UTC 28 Jul). The ensemble mean TC location at the initial time of the forecast (1200 UTC 26 Jul) is marked by the black "X".

the CTL during later periods. Nevertheless, the variables affecting the evolution of simulated TC intensity are quite numerous and complicated. These additional issues related to forecast performance are equally important but beyond the scope of this study, which focuses primarily on this new TC initialization method.

e. *Sensitivity experiments*

Many factors (such as the resolution of the model, the number of ensemble members, and the covariance inflation) can have impacts on the results of the EnKF assimilation (Zhang et al. 2006). It is believed that the optimal settings of these factors depend on properties of different models and the specific purpose of data assimilation. Regarding the TC initialization in this study, the impacts of different settings on the EnKF are evaluated by a series of sensitivity experiments. For each experiment, instead of showing detailed figures, several key quantities are averaged over the final 6 h of the initialization period. The key quantities include the forecast ensemble mean errors and spreads of the TC center position and the axisymmetric surface wind profile, which are shown to assess the performance of the EnKF initialization. The relative differences of these quantities compared to the CTL quantities in percent are listed in Table 1. The results of NONE and TK are also listed for reference.

With regard to the domain resolution, in the LOW experiment, only the coarse domain (24-km grid spacing) is used. The results show that the TC center location cannot be accurately assimilated, and thus the average forecast position error in the final 6 h of the initialization period increases by 77%. This demonstrates that correctly resolving the storm center position and the TC inner core structure is important. In contrast, in the HIGH experiment, an extra movable inner domain is added with a resolution of 2.67 km. More reasonable initial TC fields can be established in this experiment as compared to those in LOW and CTL, although more computational resources would be needed. Compared to the results in CTL, the average forecast position error slightly decreases by 4% in HIGH, whereas the average error of the forecast axisymmetric surface wind profile decreases considerably by 39%. As for the ensemble size tests, when using only 10 ensemble members (SMALL), it can be found that the ensemble mean error of the axisymmetric surface wind profile is larger (64% increase) and the position of the TC center moves irregularly (figures not shown). In contrast, when the ensemble size is doubled to 56 (BIG), the ensemble mean errors are reduced much faster than the errors in CTL (figures not shown), indicating that less integration time is needed to make the analysis field closer to the observations. However, in the final 6 h of the initialization period, when compared with CTL, BIG only leads to a 12% reduction in the average forecast position errors. The sensitivity tests of the covariance relaxation parameter (α) show that

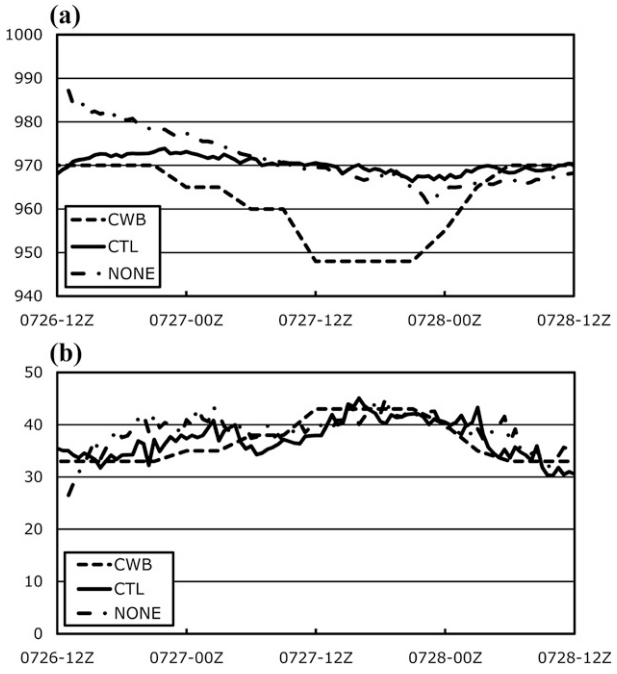

FIG. 12. The CWB observations (dashed lines) and 48-h forecast from the ensemble mean of CTL (solid lines) and NONE (dotted–dashed lines) of (a) the minimum SLP at the storm center and (b) the maximum sea surface wind speed of Typhoon Fung-wong. Both the minimum SLP and maximum sea surface wind speed are plotted at 30-min intervals.

reducing the value of α to 0.5 (ALPHA_0.5) cannot effectively prevent the excessive decrease of the background error covariance and thus leads to a continually low background error covariance (37% decrease in terms of position and 20% decrease in terms of axisymmetric surface wind profile). In contrast, the overestimated covariance inflation (ALPHA_0.95; by setting $\alpha = 0.95$) diminishes the impact of the observations on the ensemble spread so that the background error covariance increases by 57% in terms of position and by 40% in terms of the axisymmetric surface wind profile. Meanwhile, the unreasonable increase of the ensemble variance would result in significant undulations of the analysis error in the EnKF assimilation.

5. Concluding remarks

A new TC initialization method based on the EnKF is proposed in this study, which is different from the conventional methods of TC initialization (vortex bogusing, bogus data assimilation, and relocation). Three new observation operators related to the TC track and structure—center position, velocity of storm motion, and surface axisymmetric wind structure—are used to construct a reasonable initial vortex in the high-resolution WRF model. This innovative method meets two important requirements of TC initialization. First, the constructed vortex is well balanced and dynamically consistent with the numerical model. Second, the special observational TC parameters are effectively assimilated during the initialization.

The results of the initialization and simulation of the EnKF method are demonstrated in the case of Typhoon Fung-wong, with 28 ensemble members used in numerical experiments to examine the impacts of assimilating the special observational TC parameters. It is shown that the assimilation of the three special observational parameters can significantly improve the track and structure evolution of the TC during the initialization. At the end of the initialization period, a reasonable initial TC vortex is produced and can be used for follow-up simulations. In contrast, when only NCEP FNL and OISST data are adopted as the initial condition without conducting the data assimilation, the TC structure and intensity is not well developed during the first 24 h in the high-resolution WRF model run. If only the observational TC parameters associated with the TC movements are assimilated (i.e., without assimilating the mean tangential wind structure), the simulated track is consistent with the observation track during the initialization, but there is very little improvement on the TC structure. Furthermore, our experiments indicate that even when only surface wind data on a single level are assimilated, a reasonable three-dimensional vertical TC structure with the classic in–up–out secondary circulation can be successfully established by the EnKF method.

The impacts of different settings on the EnKF TC initialization, such as the resolution of the model, the number of the ensemble members, and the covariance inflation, are

TABLE 1. The average forecast ensemble mean errors and spreads of the TC center position and the axisymmetric surface wind profile during the final 6 h of the initialization period. For CTL, the actual values are listed below in boldface. For other sensitivity experiments, the relative differences as compared to CTL in percent are listed below.

	CTL	NONE (%)	TK (%)	LOW (%)	HIGH (%)	SMALL (%)	BIG (%)	ALPHA_0.5 (%)	ALPHA_0.95 (%)
Position error (km)	**13.8**	+300	−7	+77	−4	+64	−12	−12	−27
Position spread (km)	**13.5**	+304	+88	−25	+7	−22	+12	−37	+57
Wind prf. error (m s^{-1})	**1.23**	+378	+319	+52	−39	+14	+1	+24	+8
Wind prf. spread (m s^{-1})	**0.53**	+139	+43	−17	+32	−17	+6	−20	+40

studied through a series of sensitivity experiments. As expected, the higher-model-resolution run can lead to more reasonable TC initial fields although more computational resources would be needed. Regarding the impact of the ensemble size, it is found that the ensemble mean error of the axisymmetric surface wind profile is larger and the position of the TC center moves irregularly when the ensemble size is too small. In addition, the optimal value of the covariance relaxation parameter (α) in this study is found to be around 0.8. However, it is believed that the optimal settings of these factors might be dependent on properties of different models and the purpose of each data assimilation.

In all, a new method in improving the TC initialization based on the EnKF data assimilation is designed. By the EnKF method, the ensemble run of the forward nonlinear model is considered as the flow-dependent background error covariance. Many studies, such as Kalnay et al. (2007), proposed that the EnKF is comparable to 4D-VAR. However, constructing the highly nonlinear observation operator like these special TC parameters in 4D-VAR is not a simple task. This study demonstrates that the EnKF is an efficient method that makes use of available data to improve the initialization of TCs in terms of track, motion, and mean structure. Tests of this method on other stronger TCs such as Typhoon Sinlaku (2008), Krosa (2007), and Sepat (2007) have produced similar results, provided there are sufficient model resolution and spinup time. In particular, this method provides a unique opportunity to study detailed structure evolution of TCs in a high-resolution numerical model, especially when abundant data around and inside of the TC core are available. In follow-up studies (Wu et al. 2010; Huang et al. 2010), the method is applied to Typhoon Sinlaku (2008) during T-PARC, in which detailed eyewall evolution processes are examined.

Acknowledgments. The work is supported by the National Science Council of Taiwan through Grants NSC 97-2111-M-002-016-MY3 and NSC 98-2111-M-002-008-MY3, the Central Weather Bureau of Taiwan through MOTC-CWB-98-6M-01, and the Office of Naval Research Grants N00173-08-1-G007 and N000140910526.

APPENDIX

Mean Vortex Structure of Willoughby et al. (2006)

Based on 493 observed profiles, Willoughby et al. (2006) proposed sectionally continuous profiles where the wind strengthens as a power of radius inside the eye and weakens exponentially outside the eye after a smooth polynomial transition across the eyewall. The formulas used to describe the wind profile in Willoughby et al. (2006) are shown below.

$$V(r) = \begin{cases} V_i = V_{\max}\left(\dfrac{r}{R_{\max}}\right)^n, & r \le R_1 \quad \text{(A1a)} \\ V_i(1-w) + V_0 w, & R_1 < r < R_2 \quad \text{(A1b)} \\ V_0 = V_{\max}\left[(1-A)\exp\left(-\dfrac{r-R_{\max}}{X_1}\right) + A\exp\left(-\dfrac{r-R_{\max}}{X_2}\right)\right], & r \ge R_2 \quad \text{(A1c)} \end{cases}$$

$$w(\xi) = 126\xi^5 - 420\xi^6 + 540\xi^7 - 315\xi^8 + 70\xi^9,$$
$$\xi = \frac{r - R_1}{R_2 - R_1}, \quad R_1 < r < R_2 \qquad \text{(A2)}$$

$$w(\xi)|_{r=R_{\max}} = \frac{n[(1-A)X_1 + AX_2]}{n[(1-A)X_1 + AX_2] + R_{\max}}. \qquad \text{(A3)}$$

Here, V_i and V_0 are the tangential winds inside the eye and beyond the transition zone; $V_{\max}$ and $R_{\max}$ are the maximum wind and radius where the maximum wind occurs; n is the exponent for the power law inside the eye; and X_1 and X_2 are the exponents with e-folding lengths in the outer vortex, where the parameter A sets the proportion of the two exponents in the profile. In the transition zone, the weighting function w is used to ramp up smoothly from zero to one between R_1 and R_2. The extent of the transition zone is determined by satisfying the conditions shown in (A3) to assure that the maximum wind is located exactly at $R_{\max}$. Following the statistics of Willoughby et al. (2006), the fitting algorithm in this study starts with $X_2 = 40$ km, $R_1 = 0.3R_{\max}$, and

$$n = 0.4067 + 0.0144V_{\max} - 0.0038\varphi \qquad \text{(A4)}$$

to eliminate the insignificant variables, where φ is the latitude (°) of the TC.

REFERENCES

Barker, D. M., W. Huang, Y.-R. Guo, and A. J. Bourgeois, 2003: A three-dimensional variational (3DVAR) data assimilation system for use with MM5. NCAR Tech. Note NCAR/TN453+STR, 68 pp.

——, ——, ——, ——, and X. N. Xiao, 2004: A three-dimensional variational data assimilation system for MM5: Implementation and initial results. *Mon. Wea. Rev.,* **132,** 897–914.

Bender, M. A., R. J. Ross, R. E. Tuleya, and Y. Kurihara, 1993: Improvements in tropical cyclone track and intensity forecasts using the GFDL initialization system. *Mon. Wea. Rev.,* **121,** 2046–2061.

Burgers, G., P. J. van Leeuwen, and G. Evensen, 1998: Analysis scheme in the ensemble Kalman filter. *Mon. Wea. Rev.,* **126,** 1719–1724.

Chen, Y., and C. Snyder, 2007: Assimilating vortex position with an ensemble Kalman filter. *Mon. Wea. Rev.,* **135,** 1828–1845.

Chou, K.-H., and C.-C. Wu, 2008: Typhoon initialization in a mesoscale model—Combination of the bogused vortex and the dropwindsonde data in DOTSTAR. *Mon. Wea. Rev.,* **136,** 865–879.

Dudhia, J., 1989: Numerical study of convection observed during the Winter Monsoon Experiment using a mesoscale two-dimensional model. *J. Atmos. Sci.,* **46,** 3077–3107.

Edson, R. T., and M. A. Lander, 2003: A method for integrated satellite reconnaissance fix accuracy. *Extended Abstracts, 12th Conf. on Satellite Meteorology and Oceanography,* Long Beach, CA, Amer. Meteor. Soc., P2.19. [Available online at http://ams.confex.com/ams/annual2003/techprogram/paper_56946.htm.]

Elsberry, R. L., 1995: Tropical cyclone motion. Global Perspectives on Tropical Cyclones, R. Elsberry, Ed., World Meteorological Organization Rep. 693 TCP-38, 160–197.

——, and P. A. Harr, 2008: Tropical cyclone structure (TCS08) field experiment science basis, observational platforms, and strategy. *Asia-Pac. J. Atmos. Sci.,* **44,** 209–231.

Evensen, G., 1994: Sequential data assimilation with a nonlinear quasi-geostrophic model using Monte Carlo methods to forecast error statistics. *J. Geophys. Res.,* **99,** 10 143–10 162.

——, 2003: The ensemble Kalman filter: Theoretical formulation and practical implementation. *Ocean Dyn.,* **53,** 343–367.

Fujita, T., D. J. Stensrud, and D. C. Dowell, 2008: Using precipitation observations in a mesoscale short-range ensemble analysis and forecasting system. *Wea. Forecasting,* **23,** 357–372.

Gaspari, G., and S. E. Cohn, 1999: Construction of correlation functions in two and three dimensions. *Quart. J. Roy. Meteor. Soc.,* **125,** 723–757.

Grell, G. A., and D. Dévényi, 2002: A generalized approach to parameterizing convection combining ensemble and data assimilation techniques. *Geophys. Res. Lett.,* **29,** 1693, doi:10.1029/2002GL015311.

Hong, S.-Y., and J.-O. J. Lim, 2006: The WRF Single-Moment 6-Class Microphysics Scheme (WSM6). *J. Korean Meteor. Soc.,* **42,** 129–151.

——, J. Dudhia, and S.-H. Chen, 2004: A revised approach to ice microphysical processes for the bulk parameterization of clouds and precipitation. *Mon. Wea. Rev.,* **132,** 103–120.

——, Y. Noh, and J. Dudhia, 2006: A new vertical diffusion package with an explicit treatment of entrainment processes. *Mon. Wea. Rev.,* **134,** 2318–2341.

Huang, Y.-H., C.-C. Wu, J.-H. Chen, and G.-Y. Lien, 2010: Concentric eyewall formation in Typhoon Sinlaku (2008)—Part II: Dynamical analyses. *Proc. 29th Conf. on Hurricanes and Tropical Meteorology,* Tucson, AZ, Amer. Meteor. Soc., 10B.3. [Available online at http://ams.confex.com/ams/29Hurricanes/techprogram/paper_167965.htm.]

Kalnay, E., L. Hong, T. Miyoshi, S.-C. Yang, and J. Ballabrera-Poy, 2007: 4D-var or ensemble Kalman filter? *Tellus,* **59A,** 758–773.

Kurihara, Y., M. A. Bender, and R. J. Ross, 1993: An initialization scheme of hurricane models by vortex specification. *Mon. Wea. Rev.,* **121,** 2030–2045.

——, ——, R. E. Tuleya, and R. J. Ross, 1995: Improvements in the GFDL hurricane prediction system. *Mon. Wea. Rev.,* **123,** 2791–2801.

——, R. E. Tuleya, and M. A. Bender, 1998: The GFDL hurricane prediction system and its performance in the 1995 hurricane season. *Mon. Wea. Rev.,* **126,** 1306–1322.

Liu, Q., T. Marchok, H.-L. Pan, M. Bender, and S. Lord, 2002: Improvements in hurricane initialization and forecasting at NCEP with global and regional (GFDL) models. NCEP/EMC Tech. Procedures Bull. 472, 7 pp.

Mallen, K. J., M. T. Montgomery, and B. Wang, 2005: Reexamining the near-core radial structure of the tropical cyclone primary circulation: Implications for vortex resiliency. *J. Atmos. Sci.,* **62,** 408–425.

Meng, Z., and F. Zhang, 2007: Test of an ensemble Kalman filter for mesoscale and regional-scale data assimilation. Part II: Imperfect model experiments. *Mon. Wea. Rev.,* **135,** 1403–1423.

——, and ——, 2008a: Test of an ensemble Kalman filter for mesoscale and regional-scale data assimilation. Part III: Comparison with 3DVar in a real-data case study. *Mon. Wea. Rev.,* **136,** 522–540.

——, and ——, 2008b: Test of an ensemble Kalman filter for mesoscale and regional-scale data assimilation. Part IV: Comparison with 3DVar in a month-long experiment. *Mon. Wea. Rev.,* **136,** 3671–3682.

Mlawer, E. J., S. J. Taubman, P. D. Brown, M. J. Iacono, and S. A. Clough, 1997: Radiative transfer for inhomogeneous atmospheres: RRTM, a validated correlated-*k* model for the longwave. *J. Geophys. Res.,* **102,** 16 663–16 682.

Park, K., and X. Zou, 2004: Toward developing an objective 4DVAR BDA scheme for hurricane initialization based on TPC observed parameters. *Mon. Wea. Rev.,* **132,** 2054–2069.

Pu, Z.-X., and S. A. Braun, 2001: Evaluation of bogus vortex techniques with four-dimensional variational data assimilation. *Mon. Wea. Rev.,* **129,** 2023–2039.

Snyder, C., and F. Zhang, 2003: Assimilation of simulated Doppler radar observations with an ensemble Kalman filter. *Mon. Wea. Rev.,* **131,** 1663–1677.

Torn, R. D., and G. J. Hakim, 2009: Ensemble data assimilation applied to RAINEX observations of Hurricane Katrina (2005). *Mon. Wea. Rev.,* **137,** 2817–2829.

Whitaker, J. S., and T. M. Hamill, 2002: Ensemble data assimilation without perturbed observations. *Mon. Wea. Rev.,* **130,** 1913–1924.

Willoughby, H. E., R. W. R. Darling, and M. E. Rahn, 2006: Parametric representation of the primary hurricane vortex. Part II: A new family of sectionally continuous profiles. *Mon. Wea. Rev.,* **134,** 1102–1120.

Wu, C.-C., and W.-P. Huang, 2000: Numerical simulation of Typhoon Flo (1990) using a non-hydrostatic mesoscale model: The impact of initial data and initialization (in Chinese). *Atmos. Sci.,* **28,** 293–315.

——, and Coauthors, 2005: Dropwindsonde Observations for Typhoon Surveillance near the Taiwan Region (DOTSTAR): An overview. *Bull. Amer. Meteor. Soc.,* **86,** 787–790.

——, K.-H. Chou, Y. Wang, and Y.-H. Kuo, 2006: Tropical cyclone initialization and prediction based on four-dimensional variational data assimilation. *J. Atmos. Sci.,* **63,** 2383–2395.

——, G.-Y. Lien, J.-H. Chen, and Y.-H. Huang, 2010: Concentric eyewall formation in Typhoon Sinlaku (2008)—Part I: Assimilation of T-PARC data based on the ensemble Kalman filter

(EnKF). *Proc. 29th Conf. on Hurricanes and Tropical Meteorology,* Tucson, AZ, Amer. Meteor. Soc., 10B.2. [Available online at http://ams.confex.com/ams/29Hurricanes/techprogram/paper_167963.htm.]

Xiao, Q., X. Zou, and B. Wang, 2000: Initialization and simulation of a landfalling hurricane using a variational bogus data assimilation scheme. *Mon. Wea. Rev.,* **128,** 2252–2269.

Yussouf, N., and D. J. Stensrud, 2010: Impact of phased-array radar observations over a short assimilation period: Observing system simulation experiments using an ensemble Kalman filter. *Mon. Wea. Rev.,* **138,** 517–538.

Zhang, F., and C. Snyder, 2007: Ensemble-based data assimilation. *Bull. Amer. Meteor. Soc.,* **88,** 565–568.

——, ——, and J. Sun, 2004: Impacts of initial estimate and observation availability on convective-scale data assimilation with an ensemble Kalman filter. *Mon. Wea. Rev.,* **132,** 1238–1253.

——, Z. Meng, and A. Aksoy, 2006: Test of an ensemble Kalman filter for mesoscale and regional-scale data assimilation. Part I: Perfect model experiments. *Mon. Wea. Rev.,* **134,** 722–736.

——, Y. Weng, J. A. Sippel, Z. Meng, and C. H. Bishop, 2009: Cloud-resolving hurricane initialization and prediction through assimilation of Doppler radar observations with an ensemble Kalman filter: Humberto (2007). *Mon. Wea. Rev.,* **137,** 2105–2125.

Zou, X., and Q. Xiao, 2000: Studies on the initialization and simulation of a mature hurricane using a variational bogus data assimilation scheme. *J. Atmos. Sci.,* **57,** 836–860.